



Article

Assessing the Potential of IMERG and TMPA Satellite Precipitation Products for Flood Simulations and Frequency Analyses over a Typical Humid Basin in South China

Shanhu Jiang ^{1,2}, Yu Ding ², Ruolan Liu ³, Linyong Wei ², Yating Liu ², Mingming Ren ² and Liliang Ren ^{1,2,*}

¹ State Key Laboratory of Hydrology-Water Resources and Hydraulic Engineering, Hohai University, Nanjing 210098, China

² College of Hydrology and Water Resources, Hohai University, Nanjing 210098, China

³ Hangzhou Reservoir Management Service Center, Hangzhou 311122, China

* Correspondence: rll@hhu.edu.cn

Abstract: The availability of the new generation Integrated Multi-satellite Retrievals for Global Precipitation Measurement (IMERG) V06 products facilitates the utility of long-term higher spatial and temporal resolution precipitation data ($0.1^\circ \times 0.1^\circ$ and half-hourly) for monitoring and modeling extreme hydrological events in data-sparse watersheds. This study aims to evaluate the utility of IMERG Final run (IMERG-F), Late run (IMERG-L) and Early run (IMERG-E) products, in flood simulations and frequency analyses over the Mishui basin in Southern China during 2000–2017, in comparison with their predecessors, the Tropical Rainfall Measuring Mission Multi-satellite Precipitation Analysis (TMPA) products (3B42RT and 3B42V7). First, the accuracy of the five satellite precipitation products (SPPs) for daily precipitation and extreme precipitation events estimation was systematically compared by using high-density gauge station observations. Once completed, the modeling capability of the SPPs in daily streamflow simulations and flood event simulations, using a grid-based Xinanjiang model, was assessed. Finally, the flood frequency analysis utility of the SPPs was evaluated. The assessment of the daily precipitation accuracy shows that IMERG-F has the optimum statistical performance, with the highest CC (0.71) and the lowest RMSE (8.7 mm), respectively. In evaluating extreme precipitation events, among the IMERG series, IMERG-E exhibits the most noticeable variation while IMERG-L and IMERG-F display a relatively low variation. The 3B42RT exhibits a severe inaccuracy and the improvement of 3B42V7 over 3B42RT is comparatively limited. Concerning the daily streamflow simulations, IMERG-F demonstrates a superior performance while 3B42V7 tends to seriously underestimate the streamflow. With regards to the simulations of flood events, IMERG-F has performed optimally, with an average DC of 0.83. Among the near-real-time SPPs, IMERG-L outperforms IMERG-E and 3B42RT over most floods, attaining a mean DC of 0.81. Furthermore, IMERG-L performs the best in the flood frequency analyses, where bias is within 15% for return periods ranging from 2–100 years. This study is expected to contribute practical guidance to the new generation of SPPs for extreme precipitation monitoring and flood simulations as well as promoting the hydro-meteorological applications.

Keywords: satellite precipitation products; GPM IMERG; TMPA; flood simulation; flood frequency analysis



Citation: Jiang, S.; Ding, Y.; Liu, R.; Wei, L.; Liu, Y.; Ren, M.; Ren, L. Assessing the Potential of IMERG and TMPA Satellite Precipitation Products for Flood Simulations and Frequency Analyses over a Typical Humid Basin in South China. *Remote Sens.* **2022**, *14*, 4406. <https://doi.org/10.3390/rs14174406>

Academic Editor: Christopher Kidd

Received: 7 August 2022

Accepted: 2 September 2022

Published: 4 September 2022

Publisher's Note: MDPI stays neutral with regard to jurisdictional claims in published maps and institutional affiliations.



Copyright: © 2022 by the authors. Licensee MDPI, Basel, Switzerland. This article is an open access article distributed under the terms and conditions of the Creative Commons Attribution (CC BY) license (<https://creativecommons.org/licenses/by/4.0/>).

1. Introduction

Precipitation is a fundamental feature of terrestrial hydrology and contributes to the control of floods in an indispensable way [1–3]. Owing to the pronounced variability of precipitation in spatial and temporal patterns, timely and reliable acquisition of regional precipitation information is still at a bottleneck in terms of hydrological modeling and flood forecasting, particularly with regards to data-scarce and mountainous regions [4–6]. The maintenance of conventional rain gauges and ground-based radar is costly and restricted by

the topography. The new generation of multi-satellite inversion systems has facilitated the rapid acquisition of larger-scale precipitation information, which can enable the generation of instantaneous, continuous, and high-resolution three-dimensional precipitation data sets globally [7–9]. Thus, high-resolution open-access satellite precipitation products (SPPs) bring a completely new alternative data source for hydrological modeling and flood forecasting [10].

With the flourishing advancement of remote sensing technology and inversion algorithms, both spatial and temporal resolutions, as well as inversion accuracy of the new generation of SPPs have been further improved [11–13]. Among the numerous SPPs, the products of the Tropical Rainfall Measuring Mission (TRMM) Multi-satellite Precipitation Analysis (TMPA) and the Integrated Multi-satellitE Retrievals for Global Precipitation Measurement (IMERG) are the representative mainstream SPPs in recent decades. The TMPA yields reliable precipitation data in both the tropics and subtropics at a spatial resolution of $0.25^\circ \times 0.25^\circ$ and a temporal resolution of 3 h in TRMM-era [1,12]. Designed as a descendant of the TRMM, the Global Precipitation Measurement (GPM) mission is a satellite constellation mission that moves global precipitation products into a new era. The IMERG algorithm aims to produce global precipitation estimates at a spatial resolution of $0.1^\circ \times 0.1^\circ$ and at a temporal resolution of 30 min covering the full range of sensors in the TRMM and GPM eras [11]. IMERG provides three different state-of-the-art treatment modes in order to estimate precipitation, first with the 4 h latency IMERG Early Run product (IMERG-E) and followed by the 14-h latency IMERG Late Run product (IMERG-L). The final phase utilizes monthly gauge data in order to construct the research-level IMERG Final Run product with a latent duration of 3.5 months (IMERG-F). The major distinction between IMERG-E and IMERG-L is that IMERG-E contains only forward propagation (which basically amounts to extrapolation), while IMERG-L features both forward and backward propagation (allowing interpolation). The additional 10h of latency allows for lagging data transmissions to reach IMERG-L. In 2019, the IMERG V06 retrospectively created a homogeneous account of the TRMM era from 2000 (and eventually from 1998) and expanded its coverage towards both poles [14]. It is worth noting that the long-term period near real-time IMERG-E and IMERG-L products suggests their greater application utility in the hydrometeorological fields, including mesoscale and large-scale near real-time flood forecasting and drought monitoring [15–18].

Many scholars have conducted in-depth research on the performance of TMPA and IMERG products, extending from precipitation accuracy assessment to various other aspects, including hydrological simulation applications and flood forecasting [19–26]. Generally, the majority of previous studies found that TMPA and IMERG products have good potential for hydrological simulations, and that IMERG products generally perform better than TMPA products [6,17]. Wu et al. [4] established the global flood simulation monitoring system using TMPA 3B42V7 and 3B42RT as model-driven data in order to evaluate their performance in runoff simulations globally, and presented that the modeling accuracy was inferior at higher latitudes. Yuan et al. [27] evaluated the applications of multiple TRMM- and GPM-era SPPs for flood simulations at sub-daily scales in a sparsely gauged watershed in Myanmar and found that IMERG-F is a credible substitute for 3B42V7. Jiang and Bauer-Gottwein [22] examined the hydrological simulation utility of IMERG and TRMM 3B42 over 300 catchments across mainland China and concluded that IMERG outperformed TRMM 3B42 in hydrological model forcing. Zhu et al. [25] evaluated the applicability of high-temporal SPPs in flood simulations over a humid region of China and found that IMERG and TRMM were suitable for hydrological simulations at an hourly scale. However, compared with largescale research conducted on the accuracy assessment of satellite precipitation data and streamflow simulations, research on the application of SPPs in flood predictions and flood frequency analyses remains scarce. Pradhan et al. [17] reported that studies of SPPs at daily and longer time scales surpassed sub-daily ones, and highlighted the requirement for further research at a fine time resolution. Thus, there is an urgent need

to estimate and evaluate the utility of near real-time IMERG SPPs for flood simulations and frequency analyses in sub-daily resolutions.

In this context, this investigation aims to integrate a comprehensive evaluation of the hydrological utility of five sets of SPPs, TMPA 3B42RT, TMPA 3B42V7, IMERG-E, IMERG-L, and IMERG-F, in flood simulations and frequency analyses over the humid Mishui basin in South China during the period of 2000–2017. In addition to previous daily-scale precipitation evaluations and runoff simulations, the primary objectives of this study are as follows: (1) to methodically and statistically compare the accuracy of the five SPPs for the daily precipitation and heavy precipitation events estimation by using high-density station observations as benchmark data; (2) to comprehensively investigate the hydrological utility of SPPs in flood event simulations and flood frequency analyses. The outcomes of this study will contribute useful guidance for the monitoring of extreme precipitation and the simulations of flooding using new generation GPM-era SPPs, as well as promoting their hydrometeorological applications.

2. Study Area and Data

2.1. Study Area

The Mishui basin is located in the south-eastern part of Hunan Province, China, at $112^{\circ}52' \sim 113^{\circ}56' \text{E}$ and $26^{\circ}01' \sim 27^{\circ}10' \text{N}$ (Figure 1). The drainage area above the Ganxi hydrological station is approximately 9977 km^2 . The Mishui is the first-class tributary in the Xiangjiang River basin, with a length of about 296 km and an average slope drop of 1.01%. The topography of the Mishui basin is high in the southeast and low in the northwest. The basin belongs to the subtropical monsoonal humid climate, with four distinct seasons and abundant rainfall. The average annual temperature is 18.0°C and the annual average relative humidity is 80%. Furthermore, the average wind speed is 1.8 m/s and the average annual precipitation is 1561.2 mm. The basin is known to be a high flash flood hazard area. It is a suitable typical region for exploring the potential of multiple SPPs in flood simulations and frequency analyses.

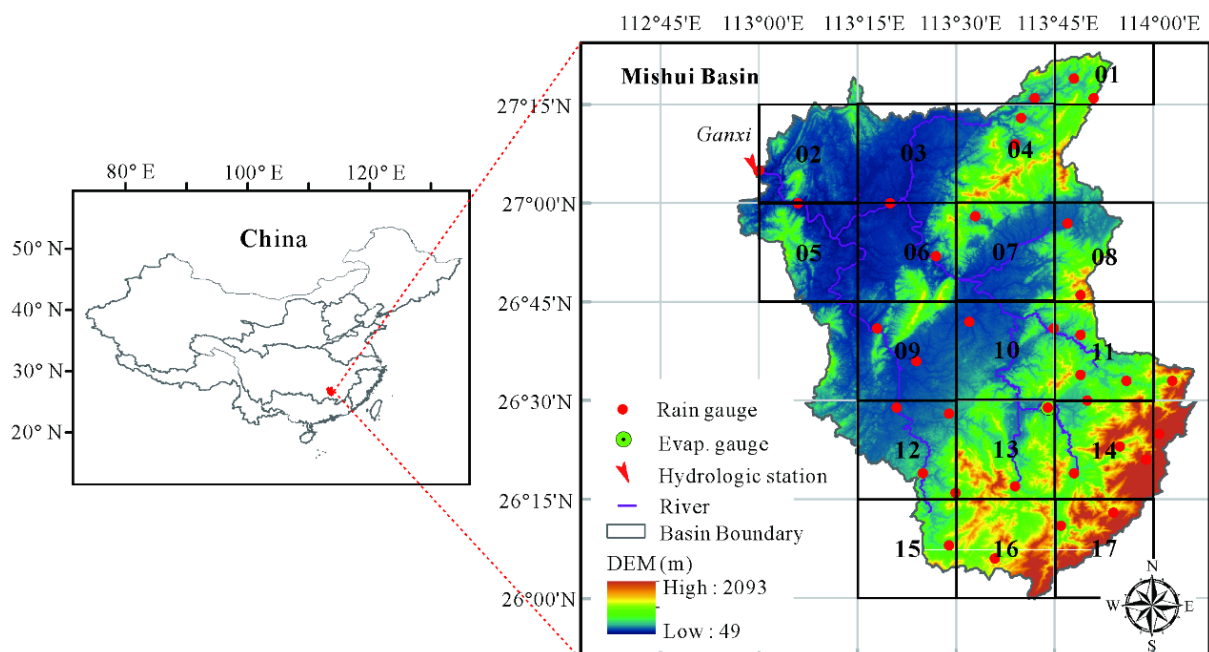


Figure 1. Digital elevation model (DEM) and spatial distribution of the rain gauge of the Mishui basin in south China.

2.2. Satellite Precipitation Products

Five SPPs, namely TMPA 3B42RT (hereafter 3B42RT), TMPA 3B42V7 (hereafter 3B42V7), IMERG-E, IMERG-L, and IMERG-F were evaluated. The TRMM is the tropical rainfall observation program of the National Aeronautics and Space Administration (NASA) and the Japan Aerospace Exploration Agency (JAXA), whose primary objective is to monitor and investigate the distribution of precipitation in the tropics [12]. The TRMM satellite precipitation data are available in four stages. The TMPA series products used in this study belong to the third stage, including the near real-time 3B42RT and the post real-time 3B42V7. The post real-time 3B42V7 integrates measured precipitation data from the Global Precipitation Climatology Centre (GPCC) ground stations for bias correction [12]. At the same time, 3B42RT has not been corrected but the errors were eliminated using the climate correction algorithm.

The GPM classifies precipitation products into four levels. The IMERG precipitation products belong to level 3; thus, all satellite microwave precipitation estimates are merged with microwave-calibrated infrared (IR) satellite estimates and precipitation gauge analyses in order to produce high resolution global SPPs [11]. Compared with the previous generation of TRMM precipitation products, the GPM delivers precipitation data with higher temporal and spatial resolution. The temporal resolution is half an hour. The spatial resolution was increased to 0.1° , implying a new era in satellite precipitation research driven by highly accurate data. The IMERG SPPs can be differentiated into three sub-products (IMERG-E (near real-time), IMERG-L (near real-time), and IMERG-F (post real-time)) based on the application of ground calibration data and their release time. IMERG-E uses only forward morphing with a latency of about 4 h while IMERG-L uses both forward and backward morphing with a latency of about 14 h. The near real-time IMERG-E and IMERG-L have no concluding calibration. In addition, IMERG-F has a latency of about 3.5 months using both forward and backward morphing and was calibrated by the GPCC. For this study, the precipitation data from June 2000 to December 2017 were used and are available for download at the official NASA website.

2.3. Gauged Precipitation and Discharge Data

The observed daily precipitation data for 2000 to 2017 were derived from 35 rain gauge stations in the Mishui basin. For the same period, the daily streamflow and potential evapotranspiration data were obtained from the Ganxi hydrological station and the Wulipai evaporation station, respectively. All data were derived from the Hydrological Bureau of the Ministry of Water Resources of China.

3. Methodology

3.1. Xinanjiang Model

The Xinanjiang Model is a conceptual model proposed by Zhao [28], which has been widely used and is particularly well-applied in the humid regions of China. In this study, a grid-based Xinanjiang (hereafter XAJ) model is proposed for daily streamflow and flood simulations. The XAJ model is mainly composed of four basic modules, namely: evapotranspiration, runoff generation, runoff delineation and flow confluence. Supported by the theory of saturation-excess runoff, the salient features of the XAJ model are the division of units, division of runoff, and division of confluence stages. Unit division refers to dividing the watershed into multiple sub-basins so as to fully reflect the spatial distribution of rainfall and the characteristics of the underlying surface of the watershed. In addition, the runoff is divided into surface runoff, soil flow, and underground runoff, according to the speed of confluence. Moreover, the division of stages means that the confluence is divided into three stages: slope confluence, river-network confluence, and channel confluence. Among them, slope confluence is calculated using the linear reservoir method, river-network confluence is calculated using the lag and route algorithm, and channel confluence is calculated using the Muskingum method. A total of 15 parameters are

included in the XAJ model, which are automatically calibrated using the global optimization algorithm (SCE-UA) developed by Duan et al. [29].

3.2. Flood Frequency Analysis

The flood frequency analysis (FFA) is crucial in statistical hydrology, which is of great significance for accurately evaluating flood risk. Although two-parameter distributions have been well developed, such as the Normal and Gumbel distributions, a number of hydrological variables are preferably characterized by three-parameter distributions, such as the Pearson type III [30]. Based on an L-moments goodness-of-fit statistic, the Pearson type III distribution was identified as a suitable distribution, which was confirmed in previous studies [31–33]. Furthermore, many studies have performed fitting analyses on the hydrological series in China, and it is believed that the P-III distribution curve provides a better fit for the rainstorm and flood series. In 2006, “Regulation for Calculating Design flood of Water Resources and Hydropower Projects” which stipulates that the P-III distribution curve is recommended for the selection of the hydrological frequency distribution (except in special cases), was published in China [34]. There are two approaches typically used for regional flood frequency analyses: annual maximum serried (AMS) and peak-over threshold (POT). The AMS uses one maximum event per year, while the POT uses every peak above the selected threshold level [35]. The AMS method is commonly adopted for recurrence intervals that are longer than 10 years since it provides statistical independence of data and focuses on small exceedance probability events [33]. Therefore, the P-III distribution was selected for the FFA in this study and the AMS model was used. The observed and modelled annual maximum peak flood discharges from 2000 to 2017 were used as input for the flood frequency analysis.

3.3. Evaluation Metrics

Five statistical indicators were identified in order to evaluate the accuracy of SPPs: correlation coefficient (CC), relative bias (Bias), root mean square error (RMSE), probability of detection (POD), and false alarm rate (FAR). The CC describes the degree of linear correlation between the satellite data and the observed data, and it ranges from 0 to 1, the closer the value is to 1, the more consistent they are. Bias shows the systematic deviation between the benchmark and satellite precipitation data. The RMSE indicates the average margin of error within the data, where a smaller value for the same benchmark reflects a higher accuracy for the data. The perfect value for the RMSE and Bias is 0. The POD and FAR are used to track the detection of precipitation events, where the POD reflects the hit rate of correctly detected rainfall events and the FAR shows the false and missing rate.

$$CC = \frac{\sum_{i=1}^n (G_i - \bar{G})(S_i - \bar{S})}{\sqrt{\sum_{i=1}^n (G_i - \bar{G})^2} \sqrt{\sum_{i=1}^n (S_i - \bar{S})^2}} \quad (1)$$

$$RMSE = \sqrt{\frac{1}{n} \sum_{i=1}^n (S_i - G_i)^2} \quad (2)$$

$$Bias = \frac{\sum_{i=1}^n (S_i - G_i)}{\sum_{i=1}^n G_i} \times 100\% \quad (3)$$

where, n is the length of the timeseries, S_i is the value of the target at time i , G_i is the value of the reference data at time i , \bar{G} and \bar{S} are the mean values.

$$POD = \frac{H}{H + M} \quad (4)$$

$$\text{FAR} = \frac{F}{H + F} \quad (5)$$

where H is the frequency of precipitation observed by both satellite and gauge, and M is the frequency of precipitation observed by gauge but not by satellite. The POD and FAR are all in the range of [0, 1] and the perfect values for the POD and FAR are 1 and 0, respectively.

In order to evaluate the accuracy of flood event simulations, GB22482-2008-T was adopted; it comprised four indicators (cumulative runoff error (REv), flood flow error (REp), error of flood time (ΔT), and determination coefficient (DC)), according to the relevant provisions of the "Hydrological Information Forecasting Standard of the People's Republic of China". The allowable error of REv and REp was 20% of the corresponding measured flow and flood flow variation; the allowable error of ΔT was 30% of the interval between the forecast time and the measured peak present time; and ± 3 h was the upper limit. DC characterizes the degree of agreement or dispersion between the flood forecast results and the measured flow with a range of [0, 1] and a perfect value of 1:

$$\text{DC} = 1 - \frac{\sum_{i=1}^n [y_c(i) - y_o(i)]^2}{\sum_{i=1}^n [y_o(i) - \bar{y}_o]^2} \quad (6)$$

where $y_c(i)$ refers to the flood forecast value, m^3/s , $y_o(i)$ refers to the observed flow value, m^3/s , \bar{y}_o is the observed flow mean value, m^3/s .

4. Result

4.1. Evaluation of Precipitation Estimations

4.1.1. Evaluation of the Daily Precipitation Estimations

Figure 2 shows the scatterplots of the daily precipitation by comparing five SPPs and rain-gauge observed precipitation. As can be noted, 3B42RT in the TMPA series of products was more divergent in the precipitation estimates, with both significant overestimation and underestimation of precipitation. Although overestimation was improved in 3B42V7, its enhancement in the underestimation of rainfall remained relatively limited. The near real-time products IMERG-E and IMERG-L performed more similarly and were also skewed in their precipitation estimates, with an apparent divergence in regions of heavy precipitation. In addition, the performance of the post real-time product IMERG-F was significantly better than that of the previous two, with further convergence of the scatter and superior agreement with station precipitation. In summary, the post-real time precipitation products (3B42V7 and IMERG-F), which were corrected based on monthly data, outperformed the near real-time products (3B42RT, IMERG-E, and IMERG-L) at the daily time scale.

Five metrics (CC, RMSE, bias, POD, and FAR) were used in order to assess the accuracy of five SPPs in the Mishui basin between June 2000 and December 2017. The statistical results are shown in Table 1, which show that IMERG-F had the best accuracy, the highest CC (0.71), the lowest RMSE (8.7), and the most elevated POD (0.87). The CC of the post real-time product 3B42V7 (0.64) was slightly higher than that of the near real-time product 3B42RT (0.61). Moreover, the CC of the post real-time product IMERG-F (0.71) was also higher than that of the near real-time product IMERG-E (0.68) and that of IMERG-L (0.66). It is worth noting that all precipitation products suffered from underestimating precipitation, except for IMERG-L, which overestimated precipitation (0.6%). In particular, 3B42V7 had a maximum negative deviation of 5.3%. The RMSE of 3B42V7 (9.2 mm) was lower than that of 3B42RT (10.2 mm), and the RMSE of IMERG-F (8.7 mm) was also lower than that of IMERG-E (9.9 mm) and IMERG-L (9.9 mm). Notably, the RMSE of 3B42RT reached 10.2 mm. Both 3B42V7 and IMERG-F also outperformed their counterparts in the POD and FAR. In general, the accuracy of the post real-time product was better than that of the near real-time product. Furthermore, the accuracy of the IMERG series product was superior to

that of the TMPA product, which was reflected in the improvement of the CC, bias, RMSE, and the POD.

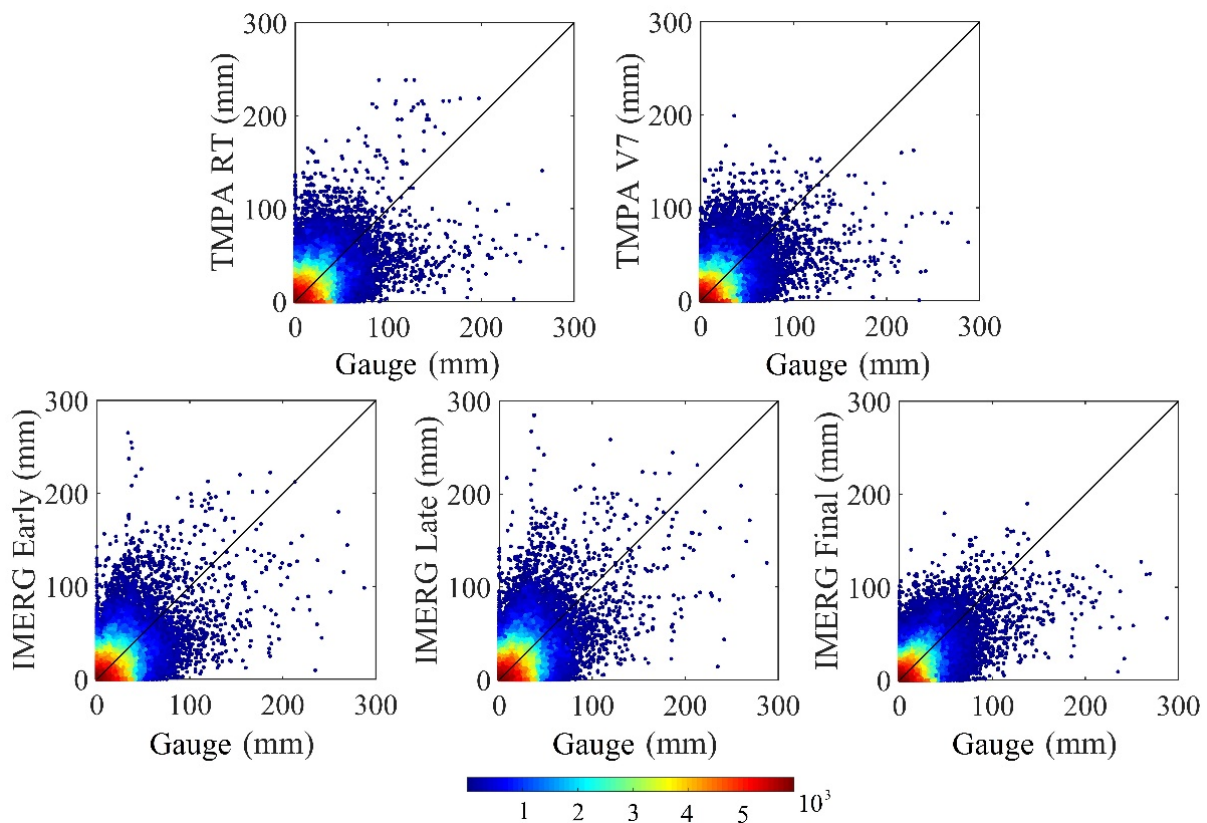


Figure 2. Scatterplots of daily precipitation comparison between five SPPs and rain-gauge observed precipitation.

Table 1. Accuracy of the evaluation metrics for the five SPPs in the Mishui Basin.

Precipitation Product	CC	Bias (%)	RMSE (mm)	POD	FAR
3B42RT	0.61	−5.2	10.2	0.57	0.23
3B42V7	0.64	−5.3	9.2	0.58	0.22
IMERG-E	0.66	−0.3	9.9	0.85	0.38
IMERG-L	0.68	0.6	9.9	0.87	0.38
IMERG-F	0.71	−1.1	8.7	0.87	0.38

A box and whisker plot of the difference between the five SPPs and the observed precipitation for different rainfall intensities under-hit conditions is provided in Figure 3. It can be seen that all five sets of SPPs exhibited an overestimation of weak precipitation events and an underestimation of heavy precipitation events. In addition, the bias towards the underestimation of precipitation worsened as the intensity of precipitation increased. When the rainfall intensity was over 100 mm/day, the underestimated deviation of precipitation was more than 50 mm. Grossly overestimated anomalies were observed above the box line plots for each precipitation product, indicating that while the SPPs presented an underestimation of precipitation overall, a gross overestimation of specific precipitation persisted. For light precipitation events (1–10 mm/day), slight overestimations existed for all precipitation products, and the deviations were relatively close. For the higher precipitation events (>25 mm/day), the variation in the deviation of the SPPs was more pronounced. In particular, for precipitation intensities above 100 mm/day, the underestimation of IMERG-L was 46.1 mm, while that of 3B42V7 was as high as 76.5 mm. In general, the devaluation of the TMPA series was more pronounced than that of the IMERG series.

The post real-time products of the same series showed a more significant underestimation than the near real-time products. Considering the significant underestimation of heavy precipitation events, improving the inversion accuracy of extreme rainfall events could serve as a direction for further improving the reliability of IMERG [36].

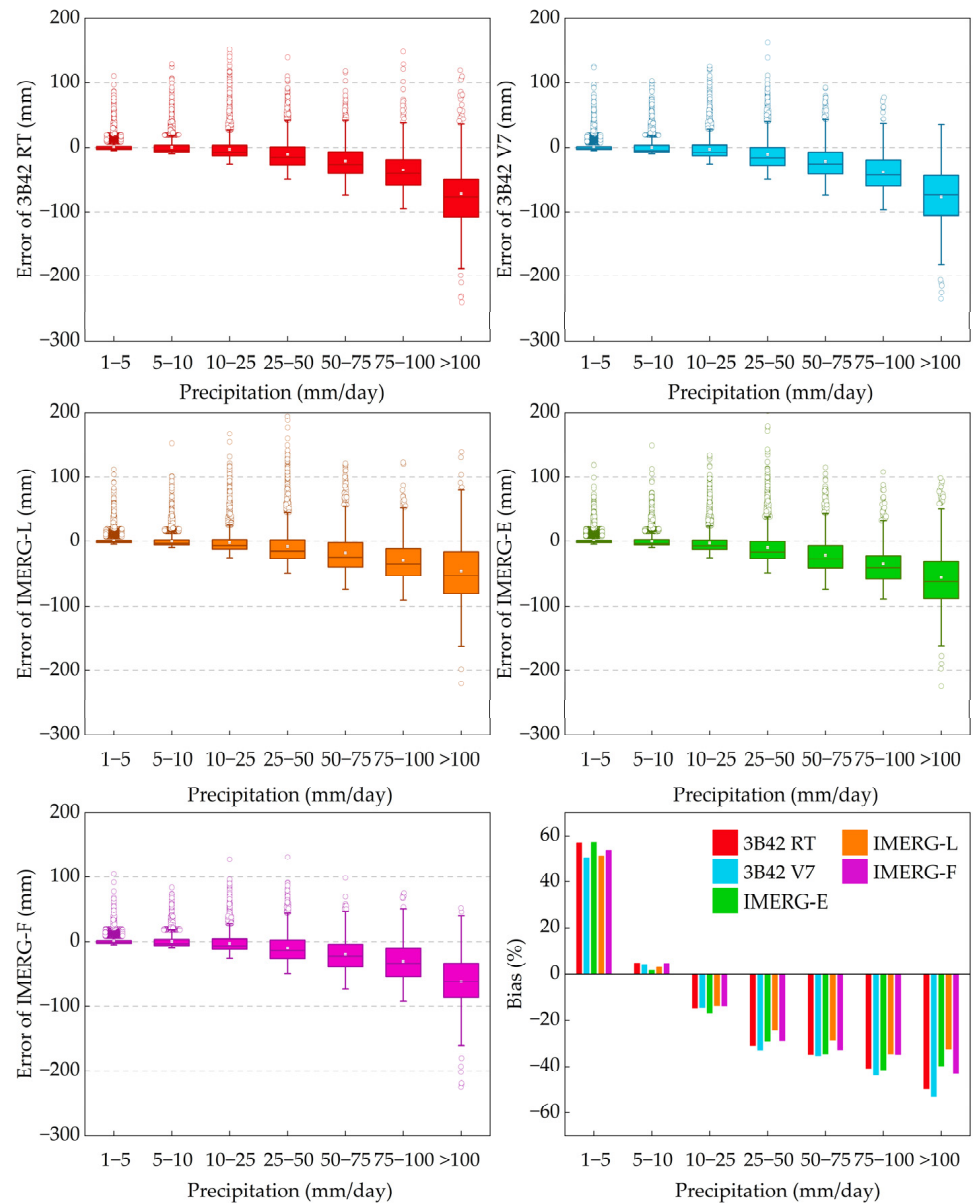


Figure 3. Boxplots of the five SPPs and the observed precipitation at different precipitation intensities. The upper and lower edges of the box mark the upper and lower quartiles (75% and 25%, respectively); the solid line in the box marks the median value; the upper and lower horizontal lines outside of the box mark the range in 1.5 IQR; the square point marks the average value; and the circular points mark the outliers.

4.1.2. Evaluation of Heavy Precipitation Events

In order to evaluate the capability of the five SPPs in monitoring extreme precipitation events more thoroughly, eight long series of heavy precipitation events were selected. The 3-hourly precipitation data from the station-observed precipitation and the TMPA series precipitation products were interpolated to 1 h. The 0.5-hourly IMERG precipitation data were accumulated to the 1-hourly scale in order to compare the precipitation variability of the different SPPs. The performance accuracy was evaluated by the CC, bias, and the RMSE.

The performance of the eight precipitation events is shown in Figure 4. It is clear that 3B42RT was not satisfactory for heavy the precipitation events estimation. The improvement in accuracy of the post real-time product 3B42V7 over 3B42RT was limited. This may be because an underestimation of heavy precipitation is more likely to occur with satellite monitoring of the precipitation. For the IMERG series, with the most significant errors and mostly negative biases, IMERG-E showed a severe underestimation of precipitation. In comparison, the deviations of IMERG-L and IMERG-F were minor. It is worth noting that the average CC of the eight heavy precipitation events in the IMERG series all reached 0.5, and the average CC of IMERG-E, IMERG-L, and IMERG-F were 0.50, 0.58, and 0.56, respectively.

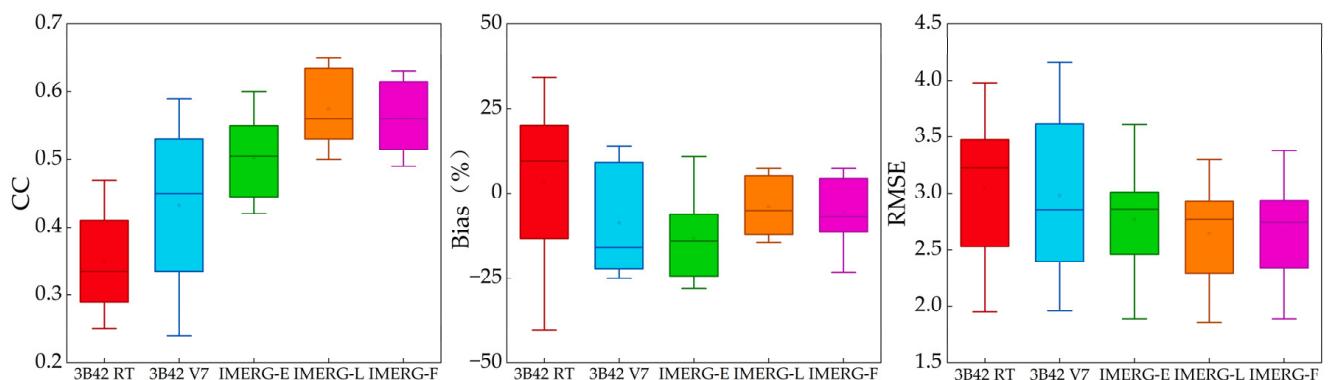


Figure 4. Boxplots of statistical metrics of eight precipitation events for the five SPPs over the Mishui basin. The upper and lower edges of the box mark the upper and lower quartiles (75% and 25%, respectively); the solid line in the box marks the median value; the upper and lower horizontal lines outside of the box mark the range in 1.5 IQR; and the square point marks the average value.

Figure 5 depicts a time series plot of the observations and the five SPPs in cumulative precipitation for different precipitation events (precipitation and flood events are named according to the corresponding dates), which shows that the trends of the SPPs were consistent with the observations, and that the SPPs could successfully capture the main precipitation process. In addition, the slopes of the precipitation accumulation lines of the different SPPs and the station were also consistent, as in the case of the two short-duration extreme precipitation events during Event 2 (20060616), indicating that the SPPs were credible in capturing extreme precipitation events. 3B42RT had the largest uncertainty and exhibited a significant overestimation of precipitation, with half overestimated and half underestimated in the eight precipitation events. In addition, the underestimation of precipitation by IMERG-E was prominent when the cumulative precipitation was high, with only one precipitation (Event 20150630), showing no significant underestimation.

In contrast, the XAJ model with the IMERG-L precipitation input effectively replicated the eight flood events, except for the events 20130514 and 20140525, which had a lower accumulative precipitation. Being a post real-time product, the performance of 3B42V7 was acceptable but inferior to IMERG-F for most flood events. The performances of IMERG-F and IMERG-L were comparable. For events 20000901 and 20070819, IMERG-F deviated more from the observed cumulative precipitation curve, while for event 20140525, IMERG-F was more consistent.

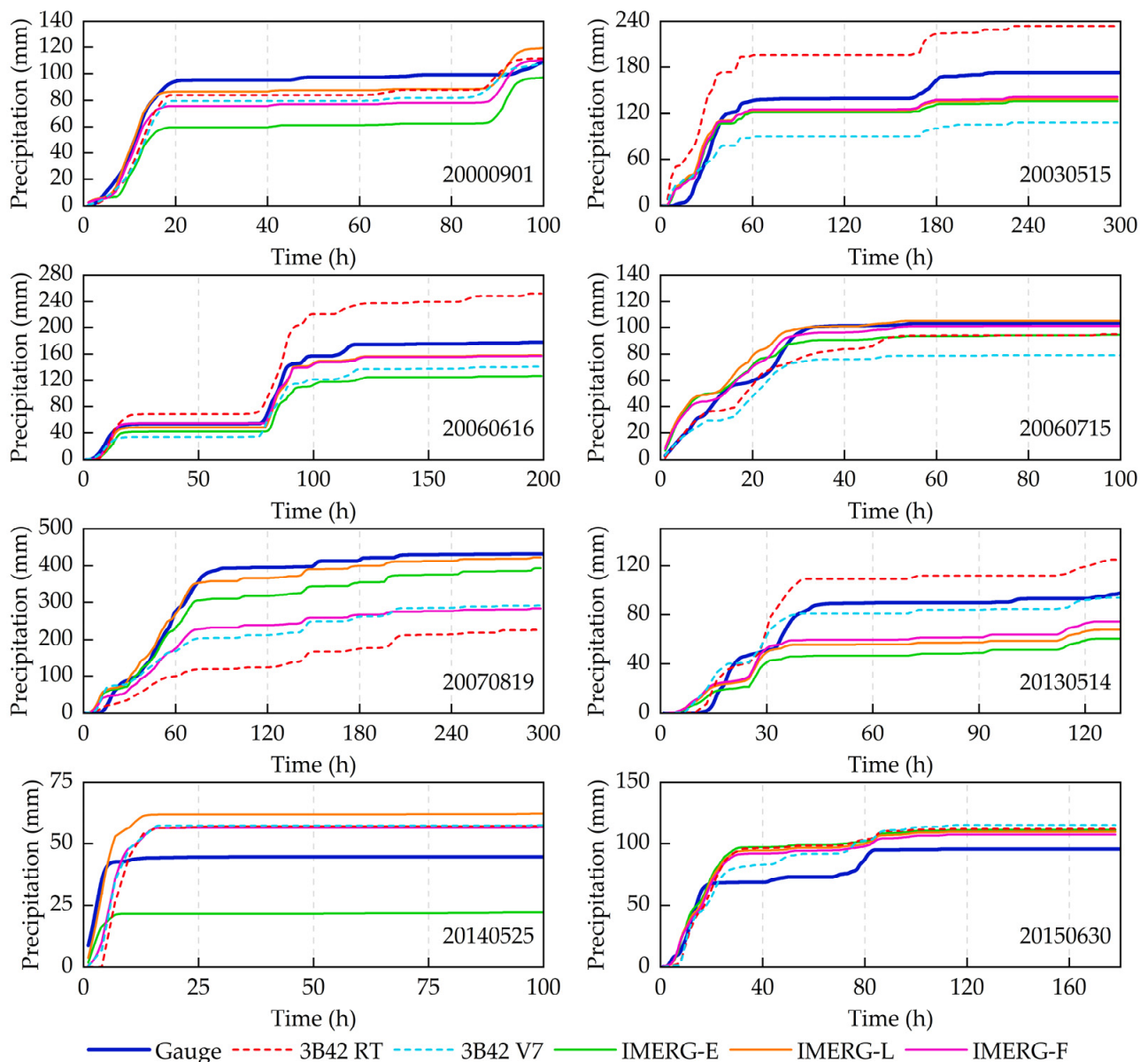


Figure 5. Comparison of the cumulative precipitation between gauge precipitation and the five SPPs of the eight historical flood events in 2000–2015 at the Ganxi hydrological station.

4.2. Evaluation of the Hydrological Utility

4.2.1. Evaluation of the Daily Streamflow Simulations

The XAJ model was applied in order to simulate the daily streamflow in the Mishui basin from June 2000 to December 2017, with 2000–2011 as the model calibration period and 2011–2017 as the model validation period. Firstly, the applicability of the XAJ model for simulating daily runoff was evaluated using rain-gauge precipitation as the model driver. The statistical results are shown in Table 2. The DC for the calibration and validation periods achieved 0.84 and 0.64, respectively, indicating the suitability of the XAJ model in the Mishui basin.

Next, the model was run from June 2000 to December 2017 using the IMERG and 3B42 products with rain gauge-calibrated model parameters. Synthetically, the post-real time IMERG-F showed the highest precision, with a DC of 0.63 and 0.55 in the calibration and validation periods, respectively. The near real-time products IMERG-E and IMERG-L had the same DC for the calibration and validation periods in the daily runoff simulations

(0.53 and 0.50, respectively). The post-real time product 3B42V7 tended to underestimate the runoff, showing a negative bias, with a deviation of no more than 3% in both the calibration and validation periods. The near real-time 3B42RT product had a CC of 0.51 for the calibration period and 0.29 for the validation period, representing the worst modeling accuracy among the five SPPs.

Table 2. Statistical results of the daily runoff during the calibration and validation periods driven by rain gauge observations and the five SPPs.

Precipitation Data	Calibration Period			Validation Period		
	CC	DC	Bias (%)	CC	DC	Bias (%)
Gauge	0.92	0.84	5.5	0.78	0.64	9.6
3B42RT	0.71	0.51	−6.0	0.70	0.29	7.8
3B42V7	0.75	0.54	−2.1	0.66	0.45	−0.8
IMERG-E	0.74	0.53	−0.1	0.62	0.50	5.7
IMERG-L	0.75	0.53	2.1	0.61	0.50	6.7
IMERG-F	0.79	0.63	0.4	0.76	0.55	0.4

Figure 6 shows the annual maximum flow series and scatterplots of the observed and simulated runoff from 2000 to 2017. Regardless of whether the precipitation observed by the rain-gauge or the precipitation from the SPPs was used as the model-driven data, the annual maximum flood peak of the runoff simulation results was found to be lower than the observed flow, which may be limited by the time scale of the precipitation data. This indicates that the SPPs estimated for extreme flood events remained imprecise on a daily scale. In addition, the underestimation of heavy precipitation by SPPs may also be the reason for the low simulated flood peak flow. Compared with the post real-time precipitation products, the three sets of near real-time precipitation products showed improvement in terms of the annual maximum runoff; however, severe overestimation and underestimation persisted.

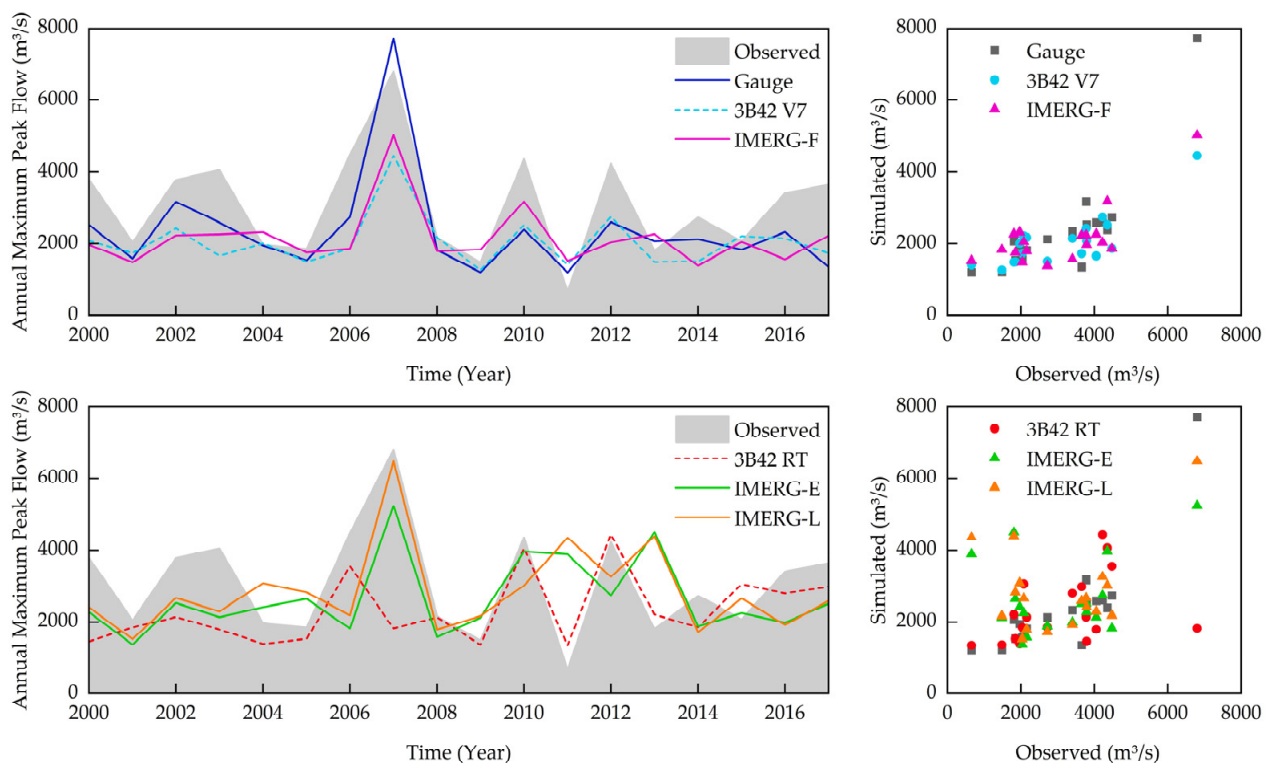


Figure 6. Selected annual peaks from the observed records and the different simulations for the period 2000–2017.

4.2.2. Evaluation of the Hourly Flood Event Simulations

The precipitation data were interpolated to a one-hour scale in order to simulate eight flood events since 2000. Five floods (20000901, 20030515, 20060616, 20060715, and 20070819) were used for calibration, and three floods (20130514, 20140525, and 20150630) were used for validation. Figure 7 depicts the comparison of the observed and simulated hourly hydrographs by gauge precipitation and the five SPPs. The detailed statistical results are provided in Table 3. The hydrological performance was quantified by the REv, REp, ΔT , and the DC.

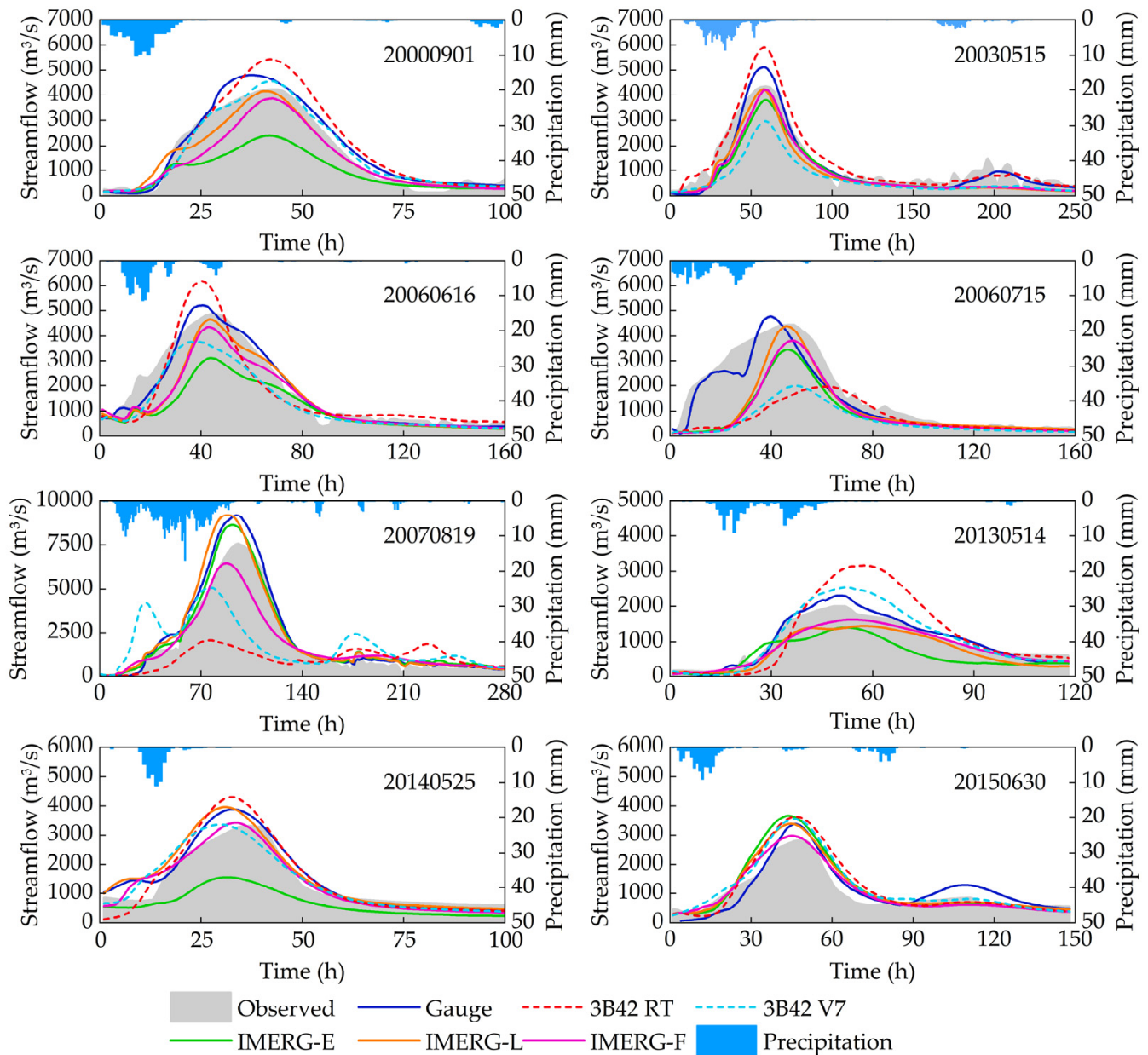


Figure 7. Comparison of the observed and simulated hourly hydrographs by gauge precipitation and the five satellite remote sensing precipitation products of the eight historical flood events in 2000–2015 at the Ganxi hydrological station.

As shown in Table 3 and Figure 7, the accuracy of each flood event simulated based on the rain-gauge was high. The DC in the calibration period reached 0.90 and the REp were all within $\pm 20\%$. The REv was within $\pm 20\%$, except for 20070819, where the REv reached 22%. Furthermore, Figure 7 indicates that the streamflow forced by the rain-gauge data

matches well with the observations. Thus, there is strong support for the applicability of the XAJ model in the Mishui Basin. The results show that 3B42RT performed poorly in event 20060715 (DC = 0.25), 20070819 (DC = 0.25), and 20130514 (DC = 0.08), implying the infeasibility of the use of 3B42RT in hourly flood event simulations. In contrast, 3B42V7 outperformed 3B42RT, with an improved DC for most events, and an average DC of 0.68. For the evaluation of the IMERG series, IMERG-E demonstrated a poor hydrological simulation, markedly underestimating the total runoff and peak flows for most events, which is inseparable from underestimating the precipitation for seven out of the eight flood events, except for event 20150630. By contrast, the accuracy of IMERG-L and IMERG-F was excellent, with a comparable performance between the two. Whereas the average DC for IMERG-L was 0.81, non-negligible deviations were observed in the simulations of runoff and flood flow in three flood events (20070819, 20130514, and 20140525), showing variations of over $\pm 20\%$ in flood flow, while three floods (20060715, 20070819, and 20130514) showed deviations of more than $\pm 20\%$ in runoff depth. The performance of IMERG-F was slightly superior to that of IMERG-L, with only one showing a REv of more than $\pm 20\%$ and all REps not exceeding $\pm 20\%$, achieving an average DC of 0.83. These results indicate that IMERG-L and IMERG-F can be utilized as an hourly scale hydrological simulation benefiting from its robustness and reliability.

Table 3. Performance of flood event simulations at the Ganxi streamflow station using the rain-gauge and the SPPs data sets.

	Gauge				3B42RT				3B42V7				IMERG-E				IMERG-L				IMERG-F			
	REv (%)	REp (%)	ΔT	DC	REv (%)	REp (%)	ΔT	DC	REv (%)	REp (%)	ΔT	DC	REv (%)	REp (%)	ΔT	DC	REv (%)	REp (%)	ΔT	DC	REv (%)	REp (%)	ΔT	DC
20000901	11.2	13.5	-2	0.94	20.9	29.1	0	0.85	-30.8	-25.8	1	0.81	-42.4	-43.2	0	0.6	-7.8	-1.5	-1	0.94	-11.6	-8.5	0	0.87
20030515	5.8	18.2	-1	0.9	35.2	36.5	-1	0.85	-36	-31.4	0	0.64	-18.7	-12.1	0	0.81	-16.7	-2.5	-2	0.87	-15.2	-2.7	0	0.85
20060616	4.4	6.6	-3	0.95	8.1	26.9	-5	0.83	-19.5	-22.8	-9	0.86	-31.8	-35.8	-1	0.65	-11.3	-4.8	-1	0.84	-12.7	-10.7	-2	0.83
20060715	-7.7	6.9	-8	0.9	-50.1	-55.9	14	0.25	-59.2	-55.2	2	0.31	-41.5	-22.2	-2	0.5	-30.7	-1.3	-2	0.56	-38.3	-14.2	0	0.52
20070819	19.3	20.9	-3	0.92	-37.8	-72.6	-19	0.21	-3.1	-33	-19	0.4	16.7	13.9	-3	0.96	20.9	21.1	-7	0.89	-4.2	-14.8	-7	0.89
20130514	7.9	15.6	2	0.93	24.5	58.6	9	0.08	9.5	27.2	3	0.78	-35.5	-30.1	3	0.61	-26.2	-28	9	0.79	-14.4	-19.4	2	0.88
20140525	9.8	17.6	-4	0.86	6.5	30.7	-4	0.77	-0.8	1.3	-7	0.87	-52.3	-52.9	-6	0.45	12.4	20	-6	0.82	-5.2	3.3	-3	0.91
20150630	20.2	19.4	-3	0.68	15.6	28.5	-1	0.61	19.3	25.8	-1	0.74	18.6	29.7	-3	0.66	14.8	19.7	-2	0.79	3.2	5.5	-2	0.89

The bias on the precipitation estimates may be exaggerated in the flood simulations. For instance, the IMERG-E product for event 20060616 was negatively biased by 21.7% for precipitation and negatively biased by 31.8% for runoff depth and 35.8% for peak flow in the corresponding flood simulation. Considering the flood simulations for five SPPs, it was concluded that the post real-time products outperformed the near real-time products of the same series. Overall, the hourly precipitation estimates from IMERG were better correlated with the ground observations than TMPA.

4.3. Evaluation of the Flood Frequency Analysis

The flood frequency analysis can provide insights into the potential of the SPPs for extreme flood event forecasting applications. The P-III distribution curve was chosen in order to calculate the design flood for the Mishui basin using the L-moment method. In Table 4, the statistical parameters of the annual maximum peak flow and design floods for different return periods based on observations and simulations of the five SPPs are presented. It is worth noting that the values of \bar{x} and Cv generated by the five SPP simulations declined in comparison with the values derived from the observations, while the Cs/Cv ratio increased. The value of \bar{x} based on the observed data is 3071.7 m³/s. Among all of the SPPs and the gauge station data, the value of \bar{x} for IMERG-L turns out to be the closest at 2848.2 m³/s. When the return period is 100, the streamflow calculated based on the observed data is 7490. The near real-time SPPs of IMERG-L, IMERG-E, and 3B42RT showed a calculated streamflow of 6811, 6133, and 5449 respectively, showing an improved performance compared with the post real-time SPPs but still exhibiting a significant underestimation.

As shown in Figure 8, the design floods for the runoff simulated based on the rain-gauge data are consistent with the observations. The results for the near real-time products

are superior to those of the same series of post real-time products (e.g., IMERG-L had a minor error in extreme floods and was close to the observed values). In contrast, the post-real time products were found to significantly underrate the design floods compared with the observation-based ones. Further, all five SPPs showed an underestimation of extreme floods, with the mean flood peak flow being lower than those observed. Concerning the relative error, the SPPs tend to overestimate floods with shorter return periods, gradually overestimating floods as the return period increased, most likely due to an overestimation of low flows and an underestimation of high flows in the runoff simulations. Among the five SPPs, IMERG-L achieved the best results, based on the determination that it fit well with the P-III distribution curve of the observed flow and was within the 15% error for return periods ranging from two to 100 years.

Table 4. Comparison of the statistical parameters and design floods between the observed and the five Satellite remote sensing precipitation products.

Data	Parameter			Return Period				
	\bar{x} (m ³ /s)	Cv	Cs/Cv	2	5	10	50	100
Observed	3071.7	0.48	2.0	2839	4196	5047	6794	7490
Gauge	2372.6	0.61	2.0	2086	3429	4312	6185	6949
TMPART	2319.1	0.41	3.0	2100	2985	3589	4904	5449
TMPAV7	2048.9	0.35	4.0	1887	2555	3007	3989	4395
IMERG-E	2656.6	0.40	3.5	2417	3406	4077	5532	6133
IMERG-L	2848.2	0.42	3.5	2566	3680	4445	6116	6811
IMERG-F	2151.9	0.38	4.0	1953	2714	3242	4401	4885

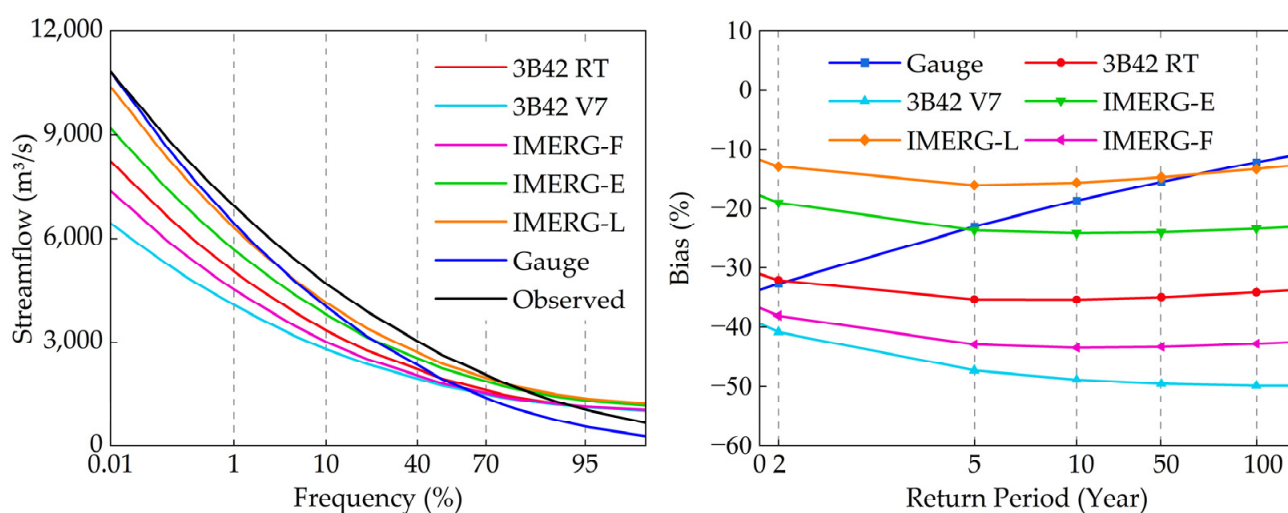


Figure 8. Comparison of the flood-frequency curves based on the observed and simulated peak flows and the bias of design floods.

5. Discussion

5.1. Comparison of the Accuracy of the SPPs

This study evaluated the reliability of five SPPs, namely IMERG-E, IMERG-L, IMERG-F, 3B42RT, and 3B42V7. Corrected based on the GPCC monthly data, IMERG-F was found to be most consistent with the rain-gauge precipitation. 3B42V7 was found to outperform 3B42RT. Overall, the accuracy of the post real-time product slightly outperformed the near real-time product, and the accuracy of the IMERG series product was superior to the TMPA product, with higher CC and RMSE values. Many studies have previously conducted the same comparative analysis in different regions and reached the same conclusions [37–41]. The detection capability at various rainfall intensities was explored in under-hit conditions.

All five SPPs revealed an overestimation of minor precipitation events and an underestimation of heavy precipitation events. With the increase in the precipitation intensity, the precipitation was underestimated in the evaluation of IMERG over mainland China [42]. It is worth noting that the underestimation of precipitation by TMPA is more severe than that of IMERG. This suggests that the underestimation of the post real-time product was greater than the near real-time product because the precipitation product was subject to both misreporting and omission errors, while the improvement in the detection probability of precipitation events was not achieved by the correction using the GPCP monthly precipitation data. As a result, in order to balance the overestimation of the rainfall due to misreporting, the correction algorithm uniformly reduced the precipitation estimate, resulting in a further underestimation under the hit scenario. In general, compared with the previous generation of TMPA precipitation products, IMERG was found to be significantly superior in all evaluation metrics.

Furthermore, the inversion evaluation of the heavy precipitation events showed distinct variations. Among the eight heavy precipitation events evaluated, 3B42RT was found to be the least effective in capturing heavy precipitation events, wherein 3B42V7 showed a similar accuracy to 3B42RT. Except for 3B42RT, all SPPs underestimated extreme precipitation events, consistent with the conclusion of the assessment in China conducted by Fang et al. [36]. Moreover, IMERG-E exhibited a severe underestimation of heavy precipitation, while IMERG-L and IMERG-F exhibited lower systematic biases and performed better. On the other hand, the IMERG family of products was found to reflect trends more accurately in heavy precipitation than TMPA, especially in the near real-time products, with IMERG-L achieving a higher CC and a lower RMSE. Moreover, for the detection capability of extreme precipitation events, the CSI indicator is proposed to be used in order to conduct a more comprehensive assessment in future studies. The near real-time precipitation products are more valuable for real-time hydrological warnings and forecasting due to their short time lag and high timeliness. The IMERG-E product was found to be less effective than the IMERG-L product, most likely because IMERG-L incorporates more passive microwave data in order to ensure more accurate precipitation estimates. Additionally, the forward projection algorithm for cloud vector motion is used in the IMERG-E product due to the differences in data algorithms, while the bi-directional algorithm formed by the increased backward algorithm is used in the IMERG-L product, which is more efficient in using microwave data. The results confirmed the higher accuracy of IMERG-F and the superior extreme precipitation detection capability of IMERG-L at the hourly scale, confirming a new basis towards the hydrological utilization of GPM-era SPPs for the Mishui Basin.

5.2. Analysis of the Hydrological Utility of SPPs

The IMERG series outperformed the TMPA series in the daily runoff simulations, with higher CC and DC values. Although IMERG-F showed the best performance, it remained inferior to those driven by the benchmark precipitation. As such, replacing gauge observations completely with the SPPs remains difficult [43]. Furthermore, the SPPs were evaluated on a 1-hourly temporal scale in this study. Yuan et al. [41] conducted an early 3-hourly flood event simulation of the IMERG and 3B42V7 using the XAJ hydrological model. They found that both the IMERG- and 3B42V7-based model runs could reproduce historical flood events in two scenarios, wherein IMERG was superior to 3B42V7. Over a humid region of China, Zhu et al. [25] found that IMERG-E, IMERG-L, and 3B42RT showed comparable performances in flood event simulations, while IMERG-E and IMERG-L performed slightly better than TRMM. Furthermore, they found that IMERG-F was more feasible for flood event simulations, with the highest NSE in most events. This study found that 3B42RT exhibited substantial uncertainties and significant over- and underestimations of precipitation, ascribing to its poor detection of precipitation, which was further amplified in the implementation of model simulations, giving rise to marked deviations in the flood simulations. The advantages of the post real-time product IMERG-F over 3B42V7 were more prominent in most flood simulations, showing that its hydrographs were more

consistent with observed data. The IMERG series performed more satisfactorily in the daily runoff simulations than the TMPA series and the simulations of flood events, both in post real-time and near real-time. These results fully illustrate and prove that the IMERG products were most suitable and effective for various hydrological research applications.

The outcomes of this study may serve as a guideline for the monitoring of extreme precipitation and the simulations of flooding using the new generation of GPM-era SPPs, as well as promoting hydrometeorological applications. However, the limitation of this study is that more intense precipitation and consequent flooding events were not identified for systematic consideration. Thus, it is recommended that more adequate extreme precipitation and flood data should be used in order to conduct extensive analyses on the hydrological utility of SPPs with a higher temporal resolution in order to obtain more representative conclusions in future studies.

6. Conclusions

This study thoroughly evaluated the utility of near- and post-real-time SPPs from TMPA and IMERG in flood simulations and frequency analyses over the Mishui basin in South China during 2000–2017. In addition to the evaluation and model application of daily precipitations, investigations of extreme precipitation events as well as flood simulations and flood frequency analyses are conducted in this study. The main conclusions are as follows:

1. IMERG-F achieved the highest daily precipitation accuracy among the five SPPs, with the highest CC (0.71), the lowest RMSE (8.7), and the best POD (0.87). Thus, when evaluating heavy precipitation events, IMERG products can more accurately reflect the precipitation process than TMPA products, especially for near real-time products. IMERG-L achieved a higher CC and a smaller RMSE and deviation. 3B42RT showed a significant error in rainfall estimation. The improvement of 3B42V7 compared with 3B42RT was limited, and the error in some events was even more unsatisfactory than 3B42RT;
2. The errors of the five SPPs evaluated under different precipitation intensities showed an overestimation of light precipitation and an underestimation of heavy precipitation. The underestimation increased with an increasing rain intensity. When the rainfall intensity was greater than 100 mm/day, all the five SPPs underestimated the precipitation from 46.1 mm to 76.5 mm, indicating a severe underestimation of the satellite products during heavy rainfall events. IMERG-L performed the best, with the least amount of devaluation. In contrast, after correction for monthly precipitation data, the post real-time products 3B42V7 and IMERG-F showed a greater deviation than their near real-time counterparts;
3. For the daily runoff simulations, the DC values of the IMERG-F product in the calibration and validation periods were 0.63 and 0.55, respectively, with a CC of 0.79 and 0.76, respectively, and a deviation of 0.4%, which was the best among the five sets of precipitation products. 3B42V7 tended to underestimate the runoff, and both the calibration period and the validation period were negatively biased. The DC of the 3B42RT product was 0.51 in the calibration period and 0.29 in the validation period, achieving the poorest accuracy;
4. For the evaluation of the flood simulations, among the post real-time products, IMERG-F performed better than 3B42V7 in most flood simulations and was more consistent with the hydrographs of the measured flow. Furthermore, the peak flow was also closer to the measured value, with an average DC of 0.83. Among the near real-time SPPs, IMERG-L performed better than IMERG-E and 3B42RT in most flood events, with an average DC of 0.81;
5. Regarding the flood frequency analysis, the five sets of SPPs all underestimated extreme floods, and the average flood peaks were lower than the observed values. The SPPs tended to overestimate floods with shorter return periods, and gradually shifted to overestimating floods as the return periods increased. Among them, IMERG-

L achieved the best performance. Compared with the measured flow design flood results, the bias in the return period of 2–100 years was within 15%.

Author Contributions: Conceptualization, S.J.; Formal analysis, R.L.; Funding acquisition, S.J. and L.R.; Methodology, L.W.; Project administration, L.R.; Resources, Y.D.; Software, Y.D.; Supervision, Y.L.; Validation, M.R.; Writing—original draft, Y.D.; Writing—review & editing, S.J. and Y.D. All authors have read and agreed to the published version of the manuscript.

Funding: This research was funded by the National Key Research and Development Program approved by Ministry of Science and Technology, China (2019YFC1510600); National Natural Science Foundation of China (51979069), the Natural Science Foundation of Jiangsu Province (BK20211202) the Fundamental Research Funds for the Central Universities (B200204029).

Data Availability Statement: The precipitation product used in this study was acquired from the National Aeronautics and Space Administration (<https://gpm.nasa.gov/GPM>, accessed on 1 September 2015).

Acknowledgments: The current study was jointly supported by the Program of Introducing Talents of Discipline to Universities by the Ministry of Education and the State Administration of Foreign Experts Affairs, China (B08048), and the Research Council of Norway (FRINATEK Project No. 274310).

Conflicts of Interest: There are no conflict of interest to declare.

References

1. Tapiador, F.J.; Turk, F.J.; Petersen, W.; Hou, A.Y.; García-Ortega, E.; Machado, L.A.T.; Angelis, C.F.; Salio, P.; Kidd, C.; Huffman, G.J.; et al. Global precipitation measurement: Methods, datasets and applications. *Atmos. Res.* **2012**, *104–105*, 70–97. [[CrossRef](#)]
2. Jiang, S.; Ren, L.; Hong, Y.; Yong, B.; Yang, X.; Yuan, F.; Ma, M. Comprehensive evaluation of multi-satellite precipitation products with a dense rain gauge network and optimally merging their simulated hydrological flows using the Bayesian model averaging method. *J. Hydrol.* **2012**, *452*, 213–225. [[CrossRef](#)]
3. Skofronick-Jackson, G.; Petersen, W.A.; Berg, W.; Kidd, C.; Stocker, E.F.; Kirschbaum, D.B.; Kakar, R.; Braun, S.A.; Huffman, G.J.; Iguchi, T.; et al. The Global Precipitation Measurement (Gpm) Mission for Science and Society. *Bull. Am. Meteorol. Soc.* **2017**, *98*, 1679–1695. [[CrossRef](#)]
4. Wu, H.; Adler, R.F.; Tian, Y.; Huffman, G.J.; Li, H.; Wang, J. Real-time global flood estimation using satellite-based precipitation and a coupled land surface and routing model. *Water Resour. Res.* **2014**, *50*, 2693–2717. [[CrossRef](#)]
5. Liu, D.; Yong, B.; Gourley, J.J.; Tian, Y.; Huffman, G.J.; Ren, L.; Hong, Y. Global View of Real-Time Trmm Multisatellite Precipitation Analysis: Implications for Its Successor Global Precipitation Measurement Mission. *Bull. Am. Meteorol. Soc.* **2015**, *96*, 283–296. [[CrossRef](#)]
6. Wei, L.Y.; Jiang, S.H.; Ren, L.L.; Wang, M.H.; Zhang, L.Q.; Liu, Y.; Yuan, F.; Yang, X.L. Evaluation of seventeen satellite-, reanalysis-, and gauge-based precipitation products for drought monitoring across mainland China. *Atmos. Res.* **2021**, *263*, 105813. [[CrossRef](#)]
7. Hou, S.; Tian, F.; Yang, L.; Hu, H.; Hou, A. How Does the Evaluation of the GPM IMERG Rainfall Product Depend on Gauge Density and Rainfall Intensity? *J. Hydrometeorol.* **2018**, *19*, 339–349. [[CrossRef](#)]
8. Sharifi, E.; Steinacker, R.; Saghafian, B. Multi time-scale evaluation of high-resolution satellite-based precipitation products over northeast of Austria. *Atmos. Res.* **2018**, *206*, 46–63. [[CrossRef](#)]
9. Wang, X.; Ding, Y.; Zhao, C.; Wang, J. Similarities and improvements of GPM IMERG upon TRMM 3B42 precipitation product under complex topographic and climatic conditions over Hexi region, Northeastern Tibetan Plateau. *Atmos. Res.* **2019**, *218*, 347–363. [[CrossRef](#)]
10. Tan, M.L.; Santo, H. Comparison of GPM IMERG, TMPA 3B42 and PERSIANN-CDR satellite precipitation products over Malaysia. *Atmos. Res.* **2018**, *202*, 63–76. [[CrossRef](#)]
11. Hou, A.Y.; Kakar, R.K.; Neeck, S.; Azarbarzin, A.A.; Kummerow, C.D.; Kojima, M.; Oki, R.; Nakamura, K.; Iguchi, T. The Global Precipitation Measurement Mission. *Bull. Am. Meteorol. Soc.* **2014**, *95*, 701–722. [[CrossRef](#)]
12. Wolff, D.B.; Nelkin, E.J.; Bolvin, D.T.; Huffman, G.J.; Adler, R.F.; Gu, G.; Hong, Y.; Bowman, K.P.; Stocker, E.F. The TRMM Multisatellite Precipitation Analysis (TMPA): Quasi-Global, Multiyear, Combined-Sensor Precipitation Estimates at Fine Scales. *J. Hydrometeorol.* **2007**, *8*, 38–55. [[CrossRef](#)]
13. Joyce, R.J.; Janowiak, J.E.; Arkin, P.A.; Xie, P.P. CMORPH: A method that produces global precipitation estimates from passive microwave and infrared data at high spatial and temporal resolution. *J. Hydrometeorol.* **2004**, *5*, 487–503. [[CrossRef](#)]
14. Tan, J.; Huffman, G.J.; Bolvin, D.T.; Nelkin, E.J. IMERG V06: Changes to the Morphing Algorithm. *J. Atmos. Ocean. Technol.* **2019**, *36*, 2471–2482. [[CrossRef](#)]

15. Tang, G.; Clark, M.P.; Papalexiou, S.M.; Ma, Z.; Hong, Y. Have satellite precipitation products improved over last two decades? A comprehensive comparison of GPM IMERG with nine satellite and reanalysis datasets. *Remote Sens. Environ.* **2020**, *240*, 111697. [[CrossRef](#)]
16. Jiang, S.; Wei, L.; Ren, L.; Xu, C.-Y.; Zhong, F.; Wang, M.; Zhang, L.; Yuan, F.; Liu, Y. Utility of integrated IMERG precipitation and GLEAM potential evapotranspiration products for drought monitoring over mainland China. *Atmos. Res.* **2021**, *247*, 105141. [[CrossRef](#)]
17. Pradhan, R.K.; Markonis, Y.; Vargas Godoy, M.R.; Villalba-Pradas, A.; Andreadis, K.M.; Nikolopoulos, E.I.; Papalexiou, S.M.; Rahim, A.; Tapiador, F.J.; Hanel, M. Review of GPM IMERG performance: A global perspective. *Remote Sens. Environ.* **2022**, *268*, 112754. [[CrossRef](#)]
18. Hsu, J.; Huang, W.R.; Liu, P.Y. Performance assessment of GPM-based near-real-time satellite products in depicting diurnal precipitation variation over Taiwan. *J. Hydrol. Reg. Stud.* **2021**, *38*, 100957. [[CrossRef](#)]
19. Yuan, F.; Zhang, L.; Win, K.; Ren, L.; Zhao, C.; Zhu, Y.; Jiang, S.; Liu, Y. Assessment of GPM and TRMM Multi-Satellite Precipitation Products in Streamflow Simulations in a Data-Sparse Mountainous Watershed in Myanmar. *Remote Sens.* **2017**, *9*, 302. [[CrossRef](#)]
20. Yang, X.; Yuan, F.; Liu, S.; Xu, C.-Y.; Ren, L.; Jiang, S. Quantifying multi-source uncertainties in multi-model predictions using the Bayesian model averaging scheme. *Hydrol. Res.* **2018**, *49*, 954–970. [[CrossRef](#)]
21. Zhang, S.; Wang, D.; Qin, Z.; Zheng, Y.; Guo, J. Assessment of the GPM and TRMM Precipitation Products Using the Rain Gauge Network over the Tibetan Plateau. *J. Meteorol. Res.* **2018**, *32*, 324–336. [[CrossRef](#)]
22. Jiang, L.; Bauer-Gottwein, P. How do GPM IMERG precipitation estimates perform as hydrological model forcing? Evaluation for 300 catchments across Mainland China. *J. Hydrol.* **2019**, *572*, 486–500. [[CrossRef](#)]
23. Le, M.-H.; Lakshmi, V.; Bolten, J.; Bui, D.D. Adequacy of Satellite-derived Precipitation Estimate for Hydrological Modeling in Vietnam Basins. *J. Hydrol.* **2020**, *586*, 124820. [[CrossRef](#)]
24. Zhu, Q.; Zhou, D.; Luo, Y.; Xu, Y.-P.; Wang, G.; Gao, X. Suitability of high-temporal satellite-based precipitation products in flood simulation over a humid region of China. *Hydrol. Sci. J.* **2020**, *66*, 104–117. [[CrossRef](#)]
25. Zhu, S.; Shen, Y.; Ma, Z. A New Perspective for Charactering the Spatio-temporal Patterns of the Error in GPM IMERG Over Mainland China. *Earth Space Sci.* **2021**, *8*, e2020EA001232. [[CrossRef](#)]
26. Dos Santos, V.; Oliveira, R.A.J.; Datok, P.; Sauvage, S.; Paris, A.; Gosset, M.; Sánchez-Pérez, J.M. Evaluating the performance of multiple satellite-based precipitation products in the Congo River Basin using the SWAT model. *J. Hydrol. Reg. Stud.* **2022**, *42*, 101168. [[CrossRef](#)]
27. Yuan, F.; Zhang, L.; Soe, K.; Ren, L.; Zhao, C.; Zhu, Y.; Jiang, S.; Liu, Y. Applications of TRMM- and GPM-Era Multiple-Satellite Precipitation Products for Flood Simulations at Sub-Daily Scales in a Sparsely Gauged Watershed in Myanmar. *Remote Sens.* **2019**, *11*, 140. [[CrossRef](#)]
28. Zhao, R. The Xinanjiang model applied in China. *J. Hydrol.* **1992**, *135*, 371–381. [[CrossRef](#)]
29. Duan, Q.; Sorooshian, S.; Gupta, V. Effective and efficient global optimization for conceptual rainfall-runoff models. *Water Resour. Res.* **1992**, *28*, 1015–1031. [[CrossRef](#)]
30. Wu, Y.-C.; Liou, J.-J.; Su, Y.-F.; Cheng, K.-S. Establishing acceptance regions for L-moments based goodness-of-fit tests for the Pearson type III distribution. *Stoch. Environ. Res. Risk Assess.* **2011**, *26*, 873–885. [[CrossRef](#)]
31. Hosking, J.R.M.; Wallis, J.R. The effect of intersite dependence on regional flood frequency analysis. *Water Resour. Res.* **1988**, *24*, 588–600. [[CrossRef](#)]
32. Igor, L.; Urošev, M.; Dolinaj, D.; Pantelić, M.; Telbisz, T.; Varga, G.; Savić, S.; Milošević, D. Regional Flood Frequency Analysis Based on L-Moment Approach (Case Study Tisza River Basin). *Water Resour.* **2019**, *46*, 853–860. [[CrossRef](#)]
33. Saf, B. Regional Flood Frequency Analysis Using L-Moments for the West Mediterranean Region of Turkey. *Water Resour. Manag.* **2008**, *23*, 531–551. [[CrossRef](#)]
34. Hydrology Bureau of Yangtze River Water Conservancy Commission, Ministry of Water Resources. Regulation for Calculating Design Flood of Water Resources and Hydropower Projects. *Minist. Water Resour.* **2006**, *99*, SL44-2006.
35. Lang, M.; Ouarda, T.; Bobee, B. Towards operational guidelines for over-threshold modeling. *J. Hydrol.* **1999**, *225*, 103–117. [[CrossRef](#)]
36. Fang, J.; Yang, W.; Luan, Y.; Du, J.; Lin, A.; Zhao, L. Evaluation of the TRMM 3B42 and GPM IMERG products for extreme precipitation analysis over China. *Atmos. Res.* **2019**, *223*, 24–38. [[CrossRef](#)]
37. Gao, Z.; Long, D.; Tang, G.; Zeng, C.; Huang, J.; Hong, Y. Assessing the potential of satellite-based precipitation estimates for flood frequency analysis in ungauged or poorly gauged tributaries of China's Yangtze River basin. *J. Hydrol.* **2017**, *550*, 478–496. [[CrossRef](#)]
38. Guo, X.; Long, D.; Zeng, Z.; Tang, G.; Yong, B.; Zhang, W.; Hong, Y. Statistical and Hydrological Comparisons between TRMM and GPM Level-3 Products over a Midlatitude Basin: Is Day-1 IMERG a Good Successor for TMPA 3B42V7? *J. Hydrometeorol.* **2016**, *17*, 121–137. [[CrossRef](#)]
39. Jiang, S.; Ren, L.; Xu, C.-Y.; Yong, B.; Yuan, F.; Liu, Y.; Yang, X.; Zeng, X. Statistical and hydrological evaluation of the latest Integrated Multi-satellite Retrievals for GPM (IMERG) over a midlatitude humid basin in South China. *Atmos. Res.* **2018**, *214*, 418–429. [[CrossRef](#)]

40. Wang, Q.; Xia, J.; She, D.; Zhang, X.; Liu, J.; Zhang, Y. Assessment of four latest long-term satellite-based precipitation products in capturing the extreme precipitation and streamflow across a humid region of southern China. *Atmos. Res.* **2021**, *257*, 105554. [[CrossRef](#)]
41. Yuan, F.; Wang, B.; Shi, C.; Cui, W.; Zhao, C.; Liu, Y.; Ren, L.; Zhang, L.; Zhu, Y.; Chen, T.; et al. Evaluation of hydrological utility of IMERG Final run V05 and TMPA 3B42V7 satellite precipitation products in the Yellow River source region, China. *J. Hydrol.* **2018**, *567*, 696–711. [[CrossRef](#)]
42. Nan, L.; Yang, M.; Wang, H.; Xiang, Z.; Hao, S. Comprehensive Evaluation of Global Precipitation Measurement Mission (GPM) IMERG Precipitation Products over Mainland China. *Water* **2021**, *13*, 3381. [[CrossRef](#)]
43. Su, J.; Li, X.; Ren, W.; Lü, H.; Zheng, D. How reliable are the satellite-based precipitation estimations in guiding hydrological modelling in South China? *J. Hydrol.* **2021**, *602*, 126705. [[CrossRef](#)]